PhotoniX

RESEARCH Open Access

Frequency-swept feedback interferometry for noncooperative-target ranging with a stand-off distance of several hundred meters

Yifan Wang[1], Xin Xu[1], Zongren Dai[1], Ziyu Hua[1], Chenxiao Lin[1], Yubin Hou[2], Qian Zhang[2], Pu Wang[2] and Yidong Tan[1*]

*Correspondence:
tanyd@tsinghua.edu.cn

[1] The State Key Laboratory of Precision Measurement Technology and Instruments, Department of Precision Instrument, Tsinghua University, Beijing 100084, China
[2] Institute of Laser Engineering, Faculty of Materials and Manufacturing, Beijing University of Technology, Beijing 100124, China

Abstract

Frequency-swept interferometry (FSI) is a powerful ranging method with high precision and immunity to ambient light. However, the stand-off distance of the current FSI-based ranging system for noncooperative targets is relatively short because the weak echo power cannot provide the needed signal-to-noise ratio (SNR). Here, we report a ranging method that combines FSI and the laser feedback technique. Compared with conventional FSI, the interference between the weak echo signal and the local oscillator occurs in the laser cavity, which enhances the signal spontaneously and then provides an improved SNR. In the experiments, the detection limit of the echo power is less than 0.1 fW, with a 1 mW probe beam. Based on the enhancement from the laser feedback technique, the system can detect a noncooperative target that is up to hundreds of meters away in space without extra optical amplifiers. On the other hand, a large stand-off distance makes the system sensitive to environmental disturbance, which degrades the ranging precision. To address this issue, an interferometry-based compensation device, which is also sensitive to weak echoes from noncooperative targets, is proposed to monitor the optical-path-length drifts and ensure accurate beat frequency recognition. Moreover, the device can record distance changes during the integration time of ranging and track a moving target precisely with improved temporal resolution. Owing to the high sensitivity and the validity of the compensation approach, the standard deviation in 10 measurements is better than 0.07 mm when targeting an aluminum sheet at approximately 152 m. Generally, with a large range, high relative precision, and low photon consumption, the novel technical scheme for laser ranging demonstrates new capabilities that promise to enable a wide range of applications, such as large equipment assembly and noncooperative-target tracking.

Keywords: Frequency-swept interferometry, Laser ranging, Laser feedback technique, Remote noncooperative targets

Introduction

The last several decades have witnessed the importance of laser ranging [1–4]. Many industrial, scientific, and military systems have sought reliable, high-precision, and non-contact methods for distance measurements. Recently, the flourishing developments of automatic driving, 3-D profilometry, and space exploration have further driven the need for absolute distance measurements [5–9]. A high-performance optical range finder has wild application prospects.

Among the existing optical methods, frequency-swept interferometry (FSI) is attractive because of its remarkable advantages. Compared with conventional time-of-flight (TOF) technology [10], FSI has an inherent immunity to ambient light through coherent detection, as well as a high resolution and precision. Different from the optical frequency comb [1], both stability and accuracy in measurements of FSI can be achieved inexpensively. Furthermore, an FSI-based ranging finder can monitor the distance and Doppler-based velocity of the target simultaneously in a single measurement [11, 12]. This is of great significance when monitoring moving targets.

With the above advantages, the study of FSI-based range finders has become popular since its inception in the 1980s [3]. Recently, many optimization techniques have been performed for range finding in terms of time consumption, precision, measuring range, and stability [13–17]. To date, a 100 kHz-level measuring rate has been realized with micrometer-scale resolution [8]. Reliable precision is guaranteed by more accurate system calibration [18] and more effective signal analysis algorithms [19, 20]. Additionally, the use of silicon photonics chips and embedded digital signal processors makes compatible and real-time measurements possible [21–23].

However, the measured target in most optical ranging methods is a corner prism or a reflector. More generally, in practice, targets to be monitored cannot reflect enough power, such as surfaces to be evaluated in manufacturing and key devices to be positioned during large equipment installations. For these noncooperative targets, the farthest detectable stand-off distance is much shorter, and the precision is lower because the weak echo power cannot provide a desirable signal intensity higher than the noise. To strengthen the signal-to-noise ratio (SNR), many efforts have been made [18, 24–26]. A direct way is to increase the probe-beam power. A high-power laser with sub-watt output has been selected as the source, and optical amplifiers have been used for probe-beam enhancement. These methods are easy to implement, especially considering the maturity of optical amplifiers, but the power consumption and system complexity are increased. Other solutions focus on decreasing the detector noise level, for example, by using an avalanche photodetector (APD) [27]. However, sufficient echo laser power is also necessary for a desirable SNR in this approach, and the usage of high-sensitivity photodetectors (PDs) increases the costs, which limits the applications. In total, a non-cooperative target restricts the ranging system in complexity, power consumption, and device costs and affects the SNR of detection. Simple structures, high echo-signal sensitivity, and low photon consumption are desirable in ranging scenarios.

Fortunately, laser feedback interferometry (LFI) can meet these requirements. Laser feedback occurs when the output light partially returns to the resonator, which induces intensity and phase modulation of the laser output [28, 29]. The weak-feedback signals (i.e., the echo signal) from targets participate in the stimulated radiation of the laser

and are enhanced spontaneously. Moreover, combined with the heterodyne modulation technique, the measurement signal can resonate with the relaxation oscillation (RO) of the laser and then be further enhanced. When the modulating frequency is close to the RO peak, the enhancement factor is up to 10^6 [30, 31]. In this regime, the SNR of the modulation signal is independent of the noise of the PD and is only limited by shot noise. The laser source in the LFI device works as an emitter, a responder, and an intrinsic amplifier. The remarkable amplification amount allows it to monitor noncooperative targets effectively and easily, and it has been applied in displacement and velocity measurements, tomography, particle detection, and other areas [32–36]. Therefore, the combination of LFI and FSI has great potential in providing weak echo-signal-detecting configurations without an extra external amplifier or highly sensitive PDs.

In this paper, we propose a laser ranging method based on frequency-swept feedback interferometry (FSFI). With ultrahigh sensitivity, the system can respond to weak echo signals and exhibits good performance in remote noncooperative target ranging, where the stand-off distance reaches hundreds of meters with a milliwatts-scale probe beam. Additionally, long-distance transmission will result in inevitable phase drift affected by the surroundings, and the drift will degrade the signal peaks, increase the error, and ultimately ruin the ranging precision. Although some methods have been proposed for drift compensation [14, 37], their effectiveness for remote noncooperative targets is poor. To improve this effectiveness, we demonstrate a quasi-common path compensation method. With this method, we achieve a relative precision of up to 1.3×10^{-6}. In total, with high echo-signal sensitivity, high relative precision, high stability, and low photon consumption, the overall performance of the FSFI ranging method shows that it has potential applications in various scenarios, including noncontact surface profiling, fiber-optic sensing, reflectometry, positioning, and tomography.

Methods

Theoretical model

Figure 1(a) depicts the configuration of the FSFI-based ranging system. The output beams of a frequency-swept laser are divided into two parts by a beam splitter (BS). One branch is for detection by a PD, while the other one, i.e., the probe beam illuminates a noncooperative target. With scattering, only a small part of the incident beam returns along the same path to the laser cavity. Then, the feedback light interferes with the local oscillator. Since the feedback light experiences an extra delay τ, which is induced by the optical path L_{ex}, a beat signal is generated in the laser cavity. When the optical frequency is swept linearly with time in a single trip, the frequency difference between the local oscillator and the feedback is constant. This beat frequency f_b is calculated in Eq. (1), where B and T are the optical frequency-swept bandwidth and period, respectively. $\alpha = 2B/T$ denotes the chirp rate. ϕ_0 stands for the light speed.

$$f_b = \frac{B}{T/2}\tau = \frac{2\alpha L_{ex}}{c} \tag{1}$$

Different from the conventional FSI-based ranging methods, FSFI removes the reference arm. Instead, the light field in the cavity functions as a reference, which reduces the

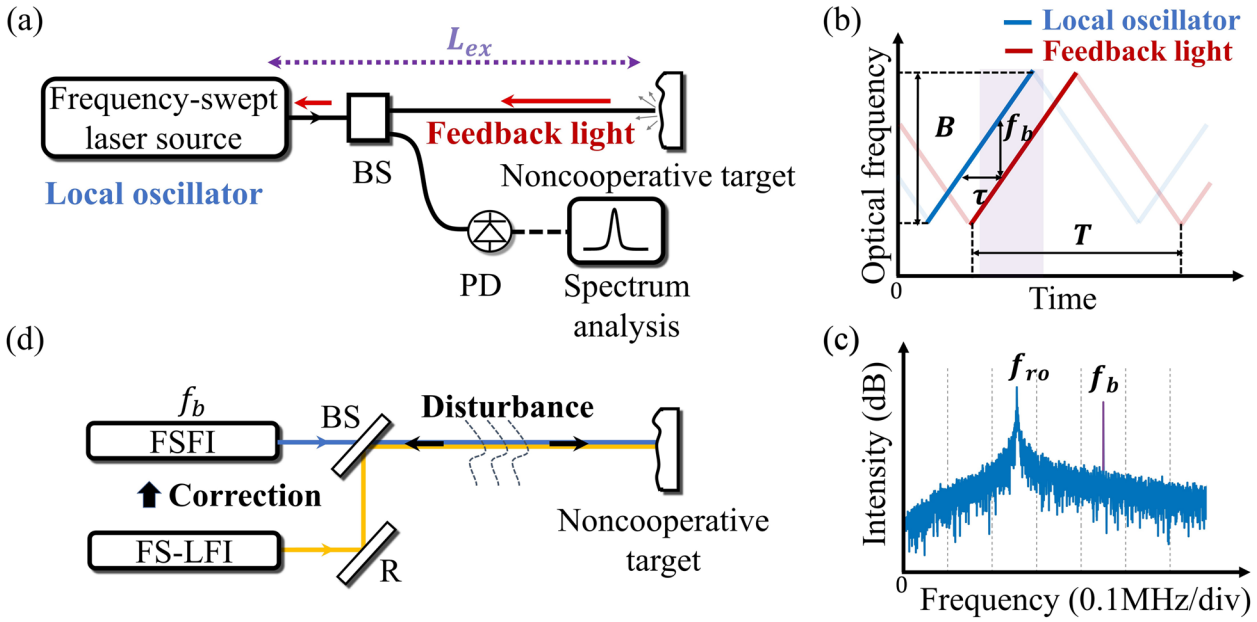

Fig. 1 **a** Principle diagram of the FSFI ranging system. BS, beam splitter; PD, photodetector; R, reflector. **b** Waveform of the swept optical frequency. **c** Typical intensity spectrum of a single-frequency fiber laser output. **d** Configuration of the FSFI ranging system with optical-path-length drift compensation

system complexity. More importantly, beam mixing inside the cavity greatly strengthens the modulation depth of the beat signal, which makes the system sensitive to weak echo signals. The weak-feedback light participates in the stimulated radiation of the laser. Similar to a perturbation, it can break up the original dynamic state of inverse populations and photons and then set up a new state. The state change in the laser significantly affects the output intensity, which can be monitored easily by a PD. The intensity response can be described as [31, 38]:

$$\frac{\Delta I(f_b)}{I} = \sqrt{R_{fb}} G(f_b) \cos\left(2\pi f_b t - \phi_0 + \Delta\phi_\tau\right) \tag{2}$$

where I is the free-running intensity. R_{fb} is the ratio of feedback power, which is proportional to the effective reflectivity of the target. ϕ_0 and $\Delta\phi_\tau$ represent the initial phase and phase related to the external cavity length L_{ex}. G is the gain factor compared with the directly detected intensity. The value of G is related to the beat frequency f_b. Particularly, if f_b is close to the RO peak frequency f_{ro} of the laser, the beat will resonate with the RO, which remarkably enhances the amplitude of the beat signal. When they coincide, G reaches its maximum. Consequently, the FSFI-based system exhibits ultrahigh detection sensitivity for weak signals from noncooperative targets. Note that the frequency of the RO depends on many factors, including the characteristics of the gain medium, cavity loss, and pump level [39]. In a single-frequency fiber laser and solid-state microchip laser [30], the typical value of the RO peak frequency is on the MHz scale, as depicted in Fig. 1(c). By analyzing the frequency spectrum of the laser output, we can obtain the enhanced beat frequency f_b and obtain the distance by Eq. (1).

High sensitivity to weak echo signals makes it possible to monitor the position of distant noncooperative targets. However, a long stand-off distance makes the impacts from the environment nonignorable. Typically, temperature fluctuations, air disturbances, and unwanted vibrations of the target induce the drift of the optical path length (OPL). As reported in [24], the drift will broaden and deviate the signal peak and finally degrades the precision. To correct it, we employ a frequency-shifted laser feedback interferometer for drift compensation (DC-LFI) to measure the OPL drift over hundreds of meters during the measurement. Moreover, DC-LFI also employs the advantage of high sensitivity and low photon consumption, which allows for the detection of remote noncooperative targets. The validity and performance of remote vibration or displacement monitoring have been reported in our previous research [32, 40]. As shown in Fig. 1(d), the probe beams from FSFI and DC-LFI are combined and propagate along the common path, and the drift affects them both. On the other hand, the signals of the two systems can be detected individually because they are from different sources. Similar to other heterodyne interferometers, the phase drift of the signal can be demodulated in DC-LFI and can be used to correct the ranging results in real time.

Experimental setup

A structural diagram of the proposed range finder for noncooperative targets is shown in Fig. 2(a). An erbium-doped distributed feedback (DFB) single-frequency fiber laser is employed as the frequency-swept source (FSS) because of its compact size and large mode-hop free range tuning. The wavelength it radiates belongs to the telecom band

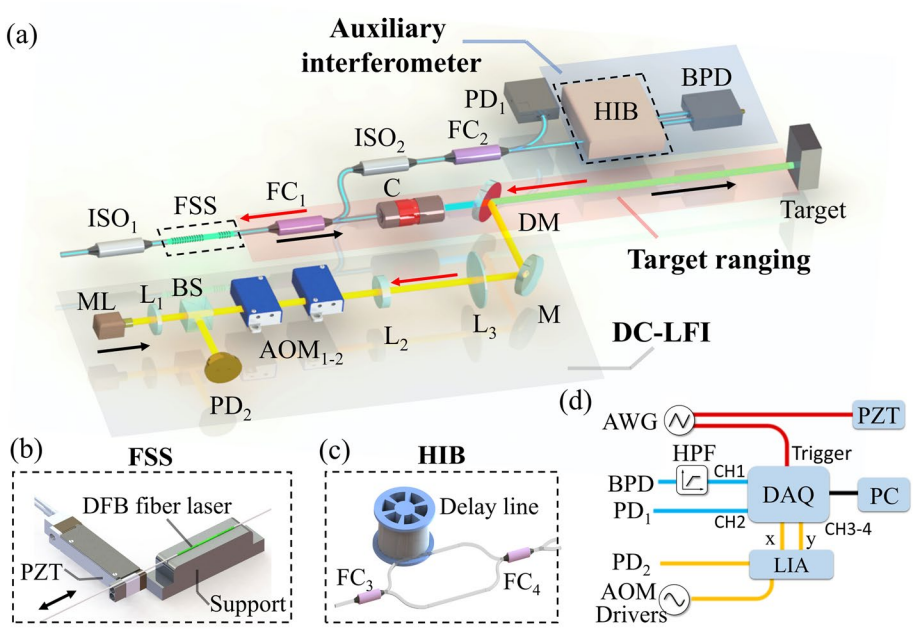

Fig. 2 Schematic diagram of the proposed FSFI ranging system with OPL drift compensation. **a** Optical design. FSS, frequency-swept source; ISO, optical isolator; FC, fiber coupler; PD, photodetector; HIB, heat insulation box; BPD, balanced photodetector; C, collimator; DM dichroic mirror; ML, microchip laser; L, lens; BS, beam splitter; AOM, acoustic-optic modulator; M, reflective mirror. The pink region marks the ranging module and illustrates the optical path to be detected. The blue- and gray-marked regions represent the auxiliary interferometer and frequency-shifted interferometer, respectively. **b** Schematic of the FSS; PZT, piezoelectric ceramic actuator. **c** Schematic of the Mach–Zehnder-type fiber interferometer in HIB. A piece of G652.D fiber is used as the delay line. **d** Schematic of the data acquisition. AWG, arbitrary waveform generator; DAQ, data acquisition card; HPF, high-pass filter; LIA, lock-in amplifier; PC, computer

around 1550 nm. The continuing advancement of fiber-optic components makes the system stable and miniaturized. Frequency swept modulation is achieved by stretching the force-preloaded laser cavity mechanically. As Fig. 2(b) shows, one end of the fiber laser is fixed on a support, and the other end is on a piezoelectric ceramic actuator (PZT, P-601.3SL, PI). The periodical motion of the PZT modulates the frequency regularly. The swept bandwidth is 200 GHz with a central wavelength of 1552 nm. More details of the laser are provided in Supplementary 1 Note 1.

The tunable DFB laser outputs 230 μW in the forward direction, and it is divided by a fiber coupler (FC_1) into two parts. One part works as the probe beam, which is collimated by a collimator, coupled out of the fiber into space, and finally illuminates a scattering target after hundreds of meters of propagation. The other part from FC_1 is for detection and analysis. One part is monitored by PD_1 through FC_2, while the other part is used as a source of the auxiliary Mach–Zehnder-type fiber interferometer, as marked in Fig. 2(a). Figure 2(c) depicts the specific configuration of the interference. According to the k-sampling technique [41, 42], the optical path difference (OPD) between the two arms is used as a standard. Therefore, we placed the two arms in a heat insulation box (HIB) to prevent the impact of ambient temperature fluctuations. The outputs of the auxiliary interferometer are detected by a balanced PD (BPD). Note that two optical isolators (ISOs) are inserted to guarantee the unidirectional propagations of nonprobe

beams and prevent parasitic optical feedbacks [43]. The parasitic feedback signals are generated by the reflective light from the interfaces of fiber-optic devices and pigtails. Without ISOs, each of them will generate a signal peak in the frequency spectrum, which may obstruct the correct peak searching in signal analysis.

Additionally, a DC-LFI is set up to compensate for the impacts of OPL drift in transmission. We use a solid-state microchip as the source with the fundamental transverse mode and single longitudinal mode. The wavelength is measured at 1064 nm. Collimated by a lens (L_1), the output is divided by a BS into two parts for detection and measurement. The reflective part is monitored by PD_2, and the transmissive part is modulated by a pair of acoustic-optic modulators (AOMs) with central frequencies of 70 MHz and 71 MHz. Selecting the specific diffractive beams, the AOMs can provide differential frequencies of $f_{\mathrm{AOM}}=1$ MHz in a single transmission and 2 MHz in a round trip. See Supplementary 1 Note 2 for more details about diffraction beam selection. The frequency-shifted beam, less than 1 mW in power, is collimated by L2 and L3, with focal lengths of -25 mm and 250 mm, respectively, to suppress the divergence. Then, the probe beam is reflected by a mirror and combined with the probe from FSFI through a dichroic mirror (DM), after which the two beams propagate along the common path to the target. With this compensation device, the phase drift can be monitored, and the stand-off distance can be obtained precisely.

Figure 2(d) shows the data acquisition of the system. A symmetry triangle wave is generated by an arbitrary waveform generator (AWG) and drives the PZT for a frequency sweep. A TTL signal synchronized with the triangle wave is used as the trigger of the data acquisition card (DAQ). The DAQ records data in four channels. Two channels are for FSFI and the auxiliary interferometer, which correspond to PD_1 and BPD, respectively. The other two are for DC-LFI and monitor the phase drift of the beam in transmission; they are demodulated by a lock-in amplifier (LIA). The reference signal of the LIA is generated by the differential driving signals of the AOMs, and the input is the detected signal from PD_2. Then, the real part, x, and the imaginary part, y, of the modulated signal are obtained and recorded by DAQ. Finally, the data are transmitted to a computer and analyzed in the frequency domain. Note that a high-pass filter (HPF) is inserted into the auxiliary signal channel. Considering that the source of the auxiliary interferometer is the same laser as the ranging module, the auxiliary signal contains the frequency components of ranging. However, the optical path of the delay line is at least twice as long as the stand-off distance, according to the Nyquist criterion in resampling. The auxiliary and ranging signals can be separated in the frequency domain, where the HPF filters the ranging signal. More details about the signal process are listed in Supplementary 1 Note 3.

Results

We set the output surface of the collimator as the zero point in ranging. Then the stand-off distance R_{mea} can be expressed as:

$$R_{mea} = \frac{L_{ex} - L_f}{n} \tag{3}$$

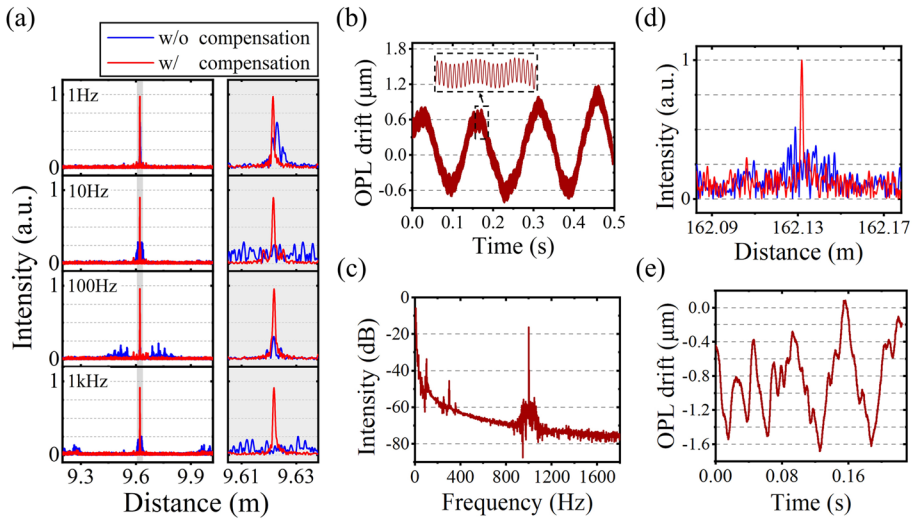

Fig. 3 Performance of the DC-LFI-based compensation method. **a** Ranging results of an aluminum sheet vibrating at 1 Hz, 10 Hz, 100 Hz, and 1 kHz with and without compensation. The right column shows the magnified details of the gray-marked parts in the left column. **b** The OPL derived by DC-LFI corresponding to the 1 kHz vibration. **c** The frequency spectrum of (**b**). **d** Ranging results with a 162.1 m stand-off distance. **e** The OPL drift recorded by DC-LFI during ranging corresponding to (**b**)

where L_f stands for the OPL in the fiber and n denotes the refractive index. A series of experiments are performed to verify the validity for ranging noncooperative targets.

Effectiveness of compensation

The performance of the compensation method based on DC-LFI is evaluated first. To simulate the OPL drift in propagation, we use a vibrating aluminum sheet as the ranging target. The effective reflectivity of the sheet is 10^{-7} and is calibrated in experiments with a Φ42.5 mm collecting aperture. The sheet is attached to another piece of PZT (Core-Morrow, Inc. XMT 150) and placed 9.6 m away from the collimator of the system. A power amplifier (Aigtek, ATA-4051) drives the sinusoidal vibration of the PZT as well as the vibration of the target, and the amplitude is on the micrometer scale. Figure 3(a) lists the ranging results with and without compensation under various frequencies from 1 Hz to 1 kHz, and the details can be seen in the right column. High-frequency components of the OPL vibration make the bandwidth of the signal obviously broaden, which leads to measurement errors. In contrast, with compensation, the signal peaks can be recognized easily but also with identical linewidths and peak positions. The proposed method is not only effective for beat-signal correction due to drifts from the Hz to kHz scale but also records the motion of the target during sweeping. Figure 3(b) shows the phase change derived by DC-LFI corresponding to the target vibration at 1 kHz. The low-frequency fluctuation originates from the ambient vibration impacts, while the high-frequency modulation in the magnified inset is generated by the PZT motion. The modulation frequency exhibited in the frequency spectrum, as shown in Fig. 3(c), coincides with the motion we impose. The effective reconstruction verifies that DC-LFI can respond to the distance change in kHz, which is much higher than the Hz-scale ranging repetition.

Another experiment is performed to test the validity of the approach in remote-target ranging. The target is 162.1 m away from the system. Figure 3(d) shows a comparison of

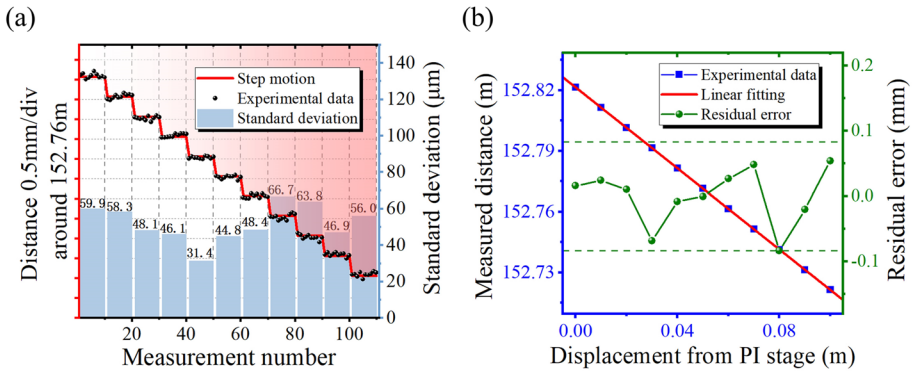

Fig. 4 Results of the precision tests. **a** The standard deviation of 10 measurements with different stand-off distances of approximately 152.76 m. The target is an aluminum sheet. **b** The linearity test results of the system

the ranging results, and Fig. 3(e) shows the corresponding OPL drift caused by environmental factors recorded by DC-LFI during measurement. The compensated signal peak, with a higher SNR and narrower bandwidth, confirms the effectiveness of our method for OPL drift compensation.

Precision and linearity

To evaluate the precision of the system, repeated measurements are conducted with OPL drift compensation. The target is the aluminum sheet mentioned above, and it is fixed on a displacement stage (PI, Inc. M511), 152.76 m away from the collimator. The measurements are repeated 10 times, and the standard deviation is calculated. Then, the stage, as well as the target, moves 500 μm in each step and 5 mm in total. For each position, similar tests are performed. The total data are displayed in Fig. 4(a), where the experimental data clearly indicate the step motion. Moreover, the standard deviation of 10 measurements in 11 positions is also analyzed. They all possess a standard deviation, σ, of no more than 0.067 mm, which corresponds to 1.3×10^{-6} relative precision, calculated by $3\sigma/R_{mea}$.

A linearity test of the system is also carried out, which demonstrates the nonlinear error in measurements. The precision of the stage is 50 nm, which can be taken as the standard. The stage drives the aluminum sheet forward by 10 cm, covering the whole travel range of the stage. Furthermore, the ranging results from FSFI are recorded. The acquired data, linear fitting results, and residual errors are marked in Fig. 4(b). The maximum residual error is 83 μm, corresponding to 8.3×10^{-4} linearity within 10 cm at 152.76 m.

Resolution

In most previous research, the resolution of the ranging system refers to the ability of the system to distinguish between several simultaneously present targets [3], and it is quantified as the full width at half the maximum (FWHM) of the signal peak. The resolution, $\Delta R = c/2B$ in theory, is determined by the frequency-swept bandwidth B. Similar tests are performed for our system. The aluminum sheet is used as the noncooperative target and is located 152 m away. The signal peak is plotted in Fig. 5(a). Numerically, the

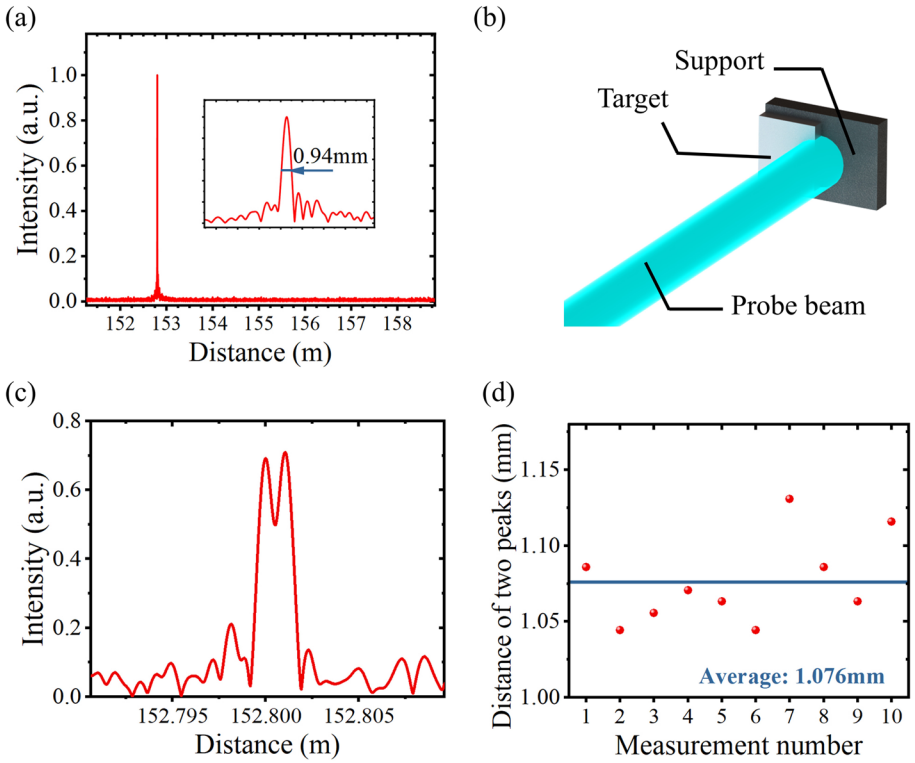

Fig. 5 Results of the resolution tests. **a** Ranging results of an aluminum sheet 152 m away from the system. Inset: magnified details of the peak. **b** Schematic diagram of the ranging targets in the resolution experiments. **c** Ranging results with two targets. **d** The gap was measured 10 times

FWHM is 0.94 mm, which is slightly worse than the theoretical value of 0.75 mm with 200 GHz tuning. This deviation originates mainly from the fiber dispersion of the delay line in the auxiliary interferometer.

In addition, we evaluate the actual resolution of the system by ranging two targets at different distances at the same time. As Fig. 5(b) shows, the probe beam illuminates the aluminum sheet and its iron support. The thickness of the sheet provides a distance difference. The ranging result is illustrated in Fig. 5 (c), where the two-peak signal is recognizable, and the resolution is realized in a real sense. In Fig. 5(d), the gap value fluctuates within 87 μm over 10 repetitions, and the average is 1.076 mm. The system resolves two noncooperative targets, even after hundreds of meters of propagation, and the experimental resolution is better than 1.1 mm.

SNR

By Eq. (1), the beat signal can be amplified in the laser cavity. On the other hand, in the band of significant amplification, the laser intensity noise (LI noise) also increases remarkably and is manifested as the RO peak. Additionally, the PD noise is another important source that contributes to the total noise. The normalized power spectra in dB of the signal and noise versus the beat frequency are shown in Fig. 6 (a). Two cases are used to analyze the SNR. (1) In the absence of PD noise, the SNR of FSFI is independent of the beat frequency and is only limited by shot noise [31], and it can be expressed as:

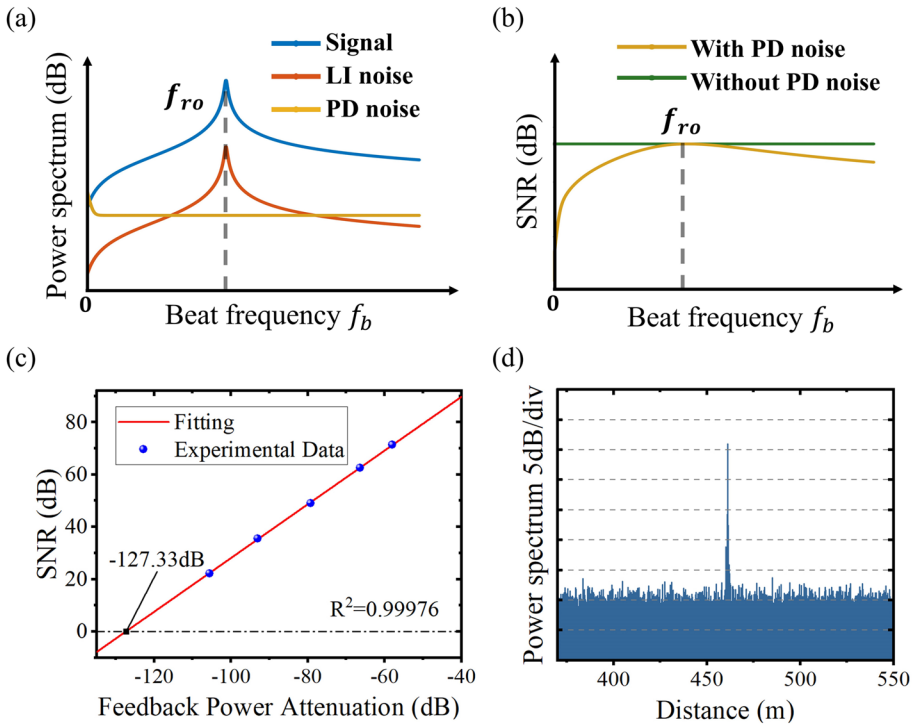

Fig. 6 SNR and detection limits of the system. **a** The normalized power spectra versus the beat frequency f_b. **b** The SNR with and without PD noise. **c** The SNR versus various feedback power attenuations. The red solid line is the linear fitting result. The black dash-dotted line is when the SNR = 1. **d** The ranging results with a 460 m stand-off distance

$$SNR_{FSFI} = \frac{PR_{fb}}{2h\nu\Delta F} \tag{4}$$

where P and ΔF represent the laser output power and demodulation bandwidth, respectively. ν is the frequency of the laser, and it can be approximated as the central frequency of sweeping. h is Planck's constant. (2) With PD noise, which is assumed to be white noise, the SNR can also reach the shot-noise limit within a frequency range close to the RO frequency, where the intensity of RO is several orders stronger than the PD noise. In this frequency band, the PD noise does not affect the SNR, even if it is much stronger than the shot noise. The SNR of the beat signal with and without PD noise is shown in Fig. 6(b). Due to the enhancement, the system eliminates the limitation caused by PD noise in the LI noise-dominating band. Beyond the band, the SNR is also enhanced and is slightly smaller in value. In total, the system exhibits ultrahigh detection sensitivity and an improved SNR for weak echo signals, even with low probe-beam power.

In our system, the noise equivalent power (NEP) of the PD is 69.5pW/Hz$^{1/2}$, which is tested in experiments. The beam power received by the PD is 22 μW, which corresponds to 2.3 pW/Hz$^{1/2}$ shot noise [44]. Compared with PD noise, shot noise hardly contributes to the total noise. In the frequency band close to the RO peak, LI noise is dominant and is up to several nW/Hz$^{1/2}$. According to the theory above, when the beat frequency f_b is located in this band, it obtains remarkable amplification, and the SNR enhancement

reaches the maximum. We evaluate the minimum detected feedback power in this regime. A cube mirror is used as the target to calibrate the power attenuation. An adjustable attenuator is installed before the collimator, which can change the optical attenuation of the probe beam. The demodulation bandwidth ΔF is 17 Hz. The SNR-attenuation curve is shown in Fig. 6(c). The slope of the fitting curve is 1.027, which verifies the linear relationship in Eq. (4). Moreover, the fitting results predict that the ideal detection limit (i.e., SNR = 1) is -127.33 dB. The output power of the laser is 230 μW, corresponding to a minimum echo power of 0.0425 fW. The theoretical detection limit is -137.22 dB, corresponding to 0.0043 fW, which is calculated by Eq. (4). The results from experiments are comparable with the theoretical results, and the experimental loss, such as a mode mismatch between the feedback beam and local oscillator, is considered.

It is verified that the proposed ranging system exhibits high sensitivity to echo signals with sub-milliwatt output power. This performance demonstrates that the system has the potential to range noncooperative targets farther. Figure 6(d) provides the results of ranging with a 460 m stand-off distance. An iron block is selected as the target, with an 8.3×10^{-7} effective reflectivity under a Φ42.5 mm collecting aperture. The signal peak is obvious compared with the noise baseline, and the SNR is over 20 dB.

Comparison with a conventional FSI-based ranging system

To make a clear comparison with a conventional FSI-based ranging system (i.e., a system without optical feedback), we perform another experiment. An FSFI-based system and a conventional FSI-based system are set up, and they target the same object under identical conditions, where they employ the same laser source, collimator, auxiliary interferometer, and detector and measure with equal probe-beam power. More details of the setup are demonstrated in Supplementary 1 Note 4. The red and black solid lines represent the PD noise and LI noise, respectively, and the LI noise is stronger than the PD noise. The power spectra of the ranging signals are shown in Fig. 7(a, b). The SNR of the conventional ranging system is 8.8 dB, while the FSFI-based SNR is 39.4 dB. The over 10^3 SNR enhancement verifies the high echo-signal sensitivity of the proposed system when the beat frequency f_b is within the LI noise-dominating frequency band.

Table 1 Characteristics of the proposed FSFI-based ranging system

Parameter	Value
Central wavelength of sweeping	1552 nm
Output power	230 μW
Minimum detectable echo power	0.043fW
Swept bandwidth	200 GHz
Stand-off distance	Hundreds of meters
Precision	3σ = 0.2 mm @152 m
Relative precision	1.3×10^{-6}
Actual resolution	1.1 mm
Sweeping frequency	~10 Hz

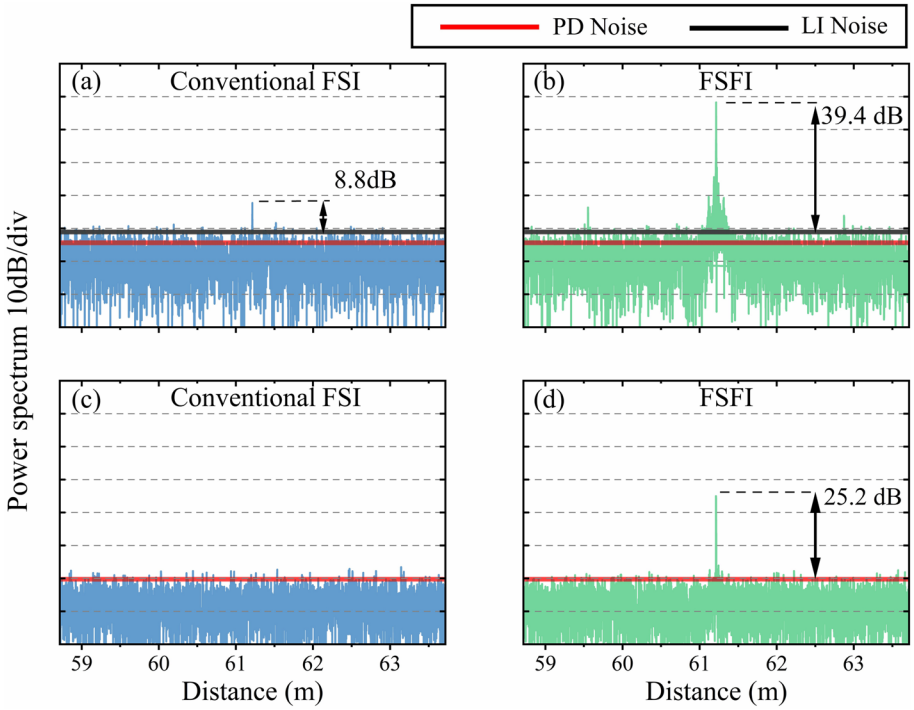

Fig. 7 Power spectra of the conventional LFI system and FSFI system in ranging. PD noise, photodetector noise. LI noise, laser intensity noise. **a**-**b** LI noise is stronger than PD noise. **c**-**d** PD noise is stronger than LI noise. **a** and **c** are the results of the conventional LFI-based ranging system. **b** and **d** are the results of the FSFI-based ranging system

Additionally, another experiment is performed when f_b is out of the LI noise-dominating band. We replace another PD with a higher NEP, where the PD noise is dominant. The power spectra of the two systems are shown in Fig. 7(c)-(d). In this case, the beat signal f_b of the conventional system is immersed in noise, while the SNR is 25.2 dB for the FSFI-based system. The results show that the FSFI also exhibits a better SNR than the conventional LFI system in the PD noise-dominating band.

Discussion

With low probe-beam power and no extra amplifier, the proposed FSFI-based ranging system achieves a stand-off-distance extension to hundreds of meters in space for noncooperative-target ranging. Additionally, the ambient impacts are addressed, which makes our system capable of obtaining a high relative precision. The performance of the system is listed in Table 1.

Condition of echo-sensitivity enhancement

The high echo sensitivity is manifested as an SNR improvement. In conventional FSI-based ranging systems, all the noise, typically the PD noise and LI noise, contributes to the gradation of the SNR. Instead, in the FSFI-based system, the resonance between the RO and the beat signal gets the SNR independent of the PD noise. Equivalently, the PD noise is remarkably suppressed when the LI noise is comparable to or stronger than the

PD noise. Therefore, FSFI works as a general PD-noise eraser, and it detects weak signals easily. Note that the premise of the intensity response enhancement in Eq. (2) is working in the weak-feedback regime [28, 45]. In this situation, the beat signal can be enhanced greatly, yet it hardly affects the laser mode or induces nonlinear oscillation. According to [46], the weak-feedback condition demands that the ratio of feedback power, R_{fb}, is less than 6×10^{-5} for the current system. This criterion can be almost met, considering that the ranging targets in our system are noncooperative and far away. See Supplementary 1 Note 5 for more details about the analysis of weak optical feedback.

Factors limiting the ranging performance

The farthest stand-off distance is determined by the minimum detectable echo power, and it is obtained in the LI-noise dominating band. By Eq. (1), the beat frequency f_b is proportional to the product of stand-off distance L_{ex} and chirp rate α. To obtain an SNR limited only by shot noise, we may need to adjust the chirp rate moderately for a feasible beat frequency. Note that even for the beat signal beyond the LI-noise dominating band, the SNR enhancement is also effective, merely slightly smaller in value. Consequently, it is not necessary to maintain the beat frequency generated by the target around the RO peak. In the experiments, the beat frequency can be 20 times larger than the RO peak, and the effective range of ranging is on the hundred-meter scale. More details of the experimental results are provided in Supplementary 1 Note 6. Therefore, the system can be used in practical scenarios where the distance to be measured can change over a large range. Additionally, adding extra optical amplifiers, a common improvement in conventional methods, is also compatible with FSFI, and they can be used to enhance the SNR and extend the stand-off distance further.

The main factor affecting the precision is the variation in the OPD between the two arms in the auxiliary interferometer. According to the k-sampling technique, the length of the OPD is regarded as the standard in ranging and should be longer than the desired maximum measurement distance by the Nyquist criterion. Since the stand-off distance in this paper exceeds 100 m, the OPD of the auxiliary interferometer is over 400 m. In the experiments, the length of the OPD is initially calibrated by a gas absorber cell (Wavelength References HCN-13-H(5.5)-25-FCAPC). However, it is difficult to keep the OPD constant during measurements because of the environmental-condition changes. For example, considering thermal expansion, the OPD variation is up to 3.4 mm/℃. Although we use an HIB to prevent disturbances from the environment, the temperature fluctuation-induced OPD drift is on the scale of tens of micrometers. If higher precision is needed, the auxiliary interferometer should be optimized or replaced by other nonlinearity correction methods, including phased locked loop, frequency comb calibration [18], and digital predistortion [47] methods.

The resolution is determined by the frequency-swept bandwidth and limited by the travel range of the PZT specifically in our system. A large tuning bandwidth demands large stretching of the DFB fiber laser cavity and correspondingly is a large driving force of the PZT. A more powerful PZT or other tunable intracavity devices, such as a Fabry–Perot filter [48], can improve the resolution. In addition, the dispersion of the delay line also extends the signal peak and decreases the resolution. This extension is proportional to the frequency-swept bandwidth. In our system, the bandwidth is relatively small.

Therefore, the dispersion-induced bandwidth increment is neglected compared with the intrinsic FWHM, ΔR. A further analysis of dispersion is demonstrated in Supplementary 1 Note 7.

Another limitation of the system is the time consumption, which relates to the realization of real-time measurements. Currently, the sweeping period determines the measuring rates, and it is limited by the PZT motion. The resonant frequency of the PZT is 322 Hz. To avoid device damage, the frequency of the triangular wave is less than 100 Hz. Overall, the swept frequency of the system is less than 60 Hz, comparable with other reported research with mechanical modulation, such as motor-based external-cavity-tunable diode lasers [49, 50]. Consequently, the usage of mechanical modulation in our system makes the ranging rate slower than electrical modulation for laser diodes (LDs). However, in LD-based FSFI systems, the sensitivity to echo signals is inferior to that of a system with a solid-state laser [51]. The trade-off is governed by the demands of specific applications.

On the other hand, the data processing time is another consumption metric. In each measurement, a few frequency components have the sample information, and others are nearly zero. Considering the size and sparsity of the data, using sparse FFT can improve the process efficiently. Other compressed sensing methods may also be used in the future. In addition, the processing is implemented in MATLAB. Rewriting the processing code in C/C++, together with GPU-accelerated parallel processing, can significantly reduce the processing time.

System complexity

The sophistication of the system mainly comes from the usage of nonlinearity-calibration or OPL drift-compensation devices, since the fundamental configuration of FSFI is compact enough. For high-precision and long-distance ranging, these correction devices are necessary to avoid beat signal degradation and ensure a correct extraction of the beat frequency. First, an auxiliary interferometer is used to correct the nonlinearity in frequency sweeping, which is a common method in the reported research [8, 9, 13]. Without closed-loop feedback control [24, 52] or other complicated devices, such as an additional laser source [12] or frequency comb [53], it is low in cost and easy to set up. Second, we use another laser source and set up DC-LFI for OPL drift compensation, and it is still effective even if the echo power from the noncooperative target is weak, or the target suffers intensive disturbance. The dual-laser configuration is also employed in the reported FSI-based ranging systems [37, 49]. Overall, compared with other methods, the methods adopted here for calibrating the nonlinearity and OPL drift are advantageous, in terms of cost and effectiveness, for noncooperative-target ranging, although they possess moderate sophistication. The system can be simplified if we employ more fiber-based or integrated devices, and this will be a focus of our future work.

DC-LFI functions in moving target tracking

Note that the usage of DC-LFI will not affect the function of tracking the position of a moving target. Figure 8(a) provides a clear description of the functions of DC-LFI. The target motion or ambient disturbance induces the OPL change, and it is monitored by

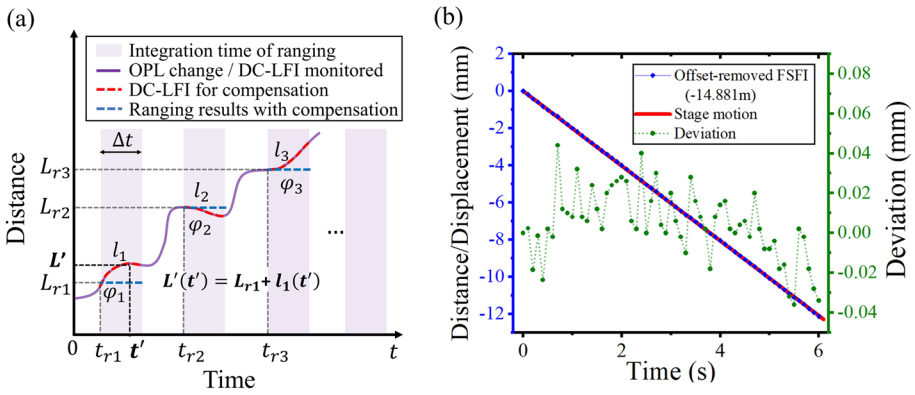

Fig. 8 Tests of moving-target monitoring. **a** The function of DC-LFI compensation. **b** Results of ranging when monitoring a moving iron block

DC-LFI. In each ranging-data acquisition window Δt, the relative phase drifts, such as $\phi_1(t)$- $\phi_1(t_{r1})$, are recorded and used to compensate for the ranging signal. With compensation, the ranging signal removes the phase change induced by the OPL change during the integration time of ranging. Therefore, the obtained ranging results are the distances (L_{r1}, L_{r2}, ...), at which the target is located when data acquisition starts (t_{r1}, t_{r2}, ...). Furthermore, the consequent motion information (l_1, l_2, ...) during the time of ranging can be derived by the relative phase drifts of the DC-LFI system, and the absolute distance can be derived in real time by adding the relative motion to the ranging results, for example, $L'(t') = L_{r1} + l_1(t')$. Since the integration time of DC-LFI is much shorter than that of ranging, the usage of DC-LFI can improve the temporal resolution of moving-target monitoring, which has been verified in Fig. 3(a-c). Consequently, the proposed system can track the position of the target precisely and nearly in real time. By comparison, the conventional method merely provides an averaged result over the integration time in each measurement.

As proof, tracking a moving target is accomplished in the experiments, and an iron block is fixed on a moving stage 14.88 m away from the system with a speed of 2 mm/s. The frequency of sweeping is set to 10 Hz. The motion of the stage is monitored by an interferometer. As Fig. 8(b) shows, the drift compensated ranging results almost coincide with the motion of the target with only a deviation of tens-of-micrometers.

Conclusions

In conclusion, an FSFI-based laser ranging system is developed. Owing to the laser feedback configuration, the ranging signal resonates with the RO and then is enhanced spontaneously. In this regime, the significant enhancement provides an improved SNR and makes remote noncooperative-target ranging possible. In the experiments, the stand-off distance is up to hundreds of meters, while the probe-beam power is approximately 1 mW. The high sensitivity of the laser feedback technique is also employed for OPL drift compensation, DC-LFI, to improve the precision of ranging. The performance tests demonstrate the necessity and validity of the compensation approach. With it, the system exhibits a precision that is better than 0.2 mm and an actual resolution that is better than 1.1 mm. Moreover, the use of

DC-LFI makes it possible to monitor the target motion precisely during the integration time of ranging. Compared with the conventional FSI-based system, the advantages of the proposed system can be summarized as high echo-signal sensitivity, high relative precision, a large range of ranging, and lower photon consumption. These features provide an extra scheme for remote-target ranging. Although there is much to improve including the resolution and measuring rate, the optimized sensor promises a wider prospect in scientific and industrial applications including 3-D profilometry, large equipment assembly, and space exploration.

Abbreviations

FSI	Frequency-swept interferometry
SNR	Signal-to-noise ratio
TOF	Time-of-flight
APD	Avalanche photodetector
LFI	Laser feedback interferometry
RO	Relaxation osculation
PD	Photodetector
FSFI	Frequency-swept feedback interferometry
BS	Beam splitter
OPL	Optical path length
DC-LFI	Laser feedback interferometer for the drift compensation
DFB	Distributed feedback
FSS	Frequency-swept source
PZT	Piezoelectric ceramic actuator
FC	Fiber coupler
OPD	Optical path difference
HIB	Heat insulation box
BPD	Balanced photodetector
ISO	Isolator
L	Lens
AOM	Acoustic-optic modulator
DM	Dichroic mirror
AWG	Arbitrary waveform generator
DAQ	Data acquisition card
LIA	Lock-in amplifier
HPF	High-pass filter
FWHM	Full width at half maximum
LI	laser intensity
NEP	Noise equivalent power
LD	Laser diode

Supplementary Information

The online version contains supplementary material available at https://doi.org/10.1186/s43074-022-00067-z.

Additional file 1. Frequency-swept feedback interferometry for noncooperative-target ranging with the stand-off distance of several hundred meters: supplemental material.

Acknowledgements

The authors gratefully acknowledge the team of Prof. F Zhang from Tianjin University and the team of Prof. G Liu from Harbin Institute of Technology for technical support.

Authors' contributions

YW and YT proposed the framework of this research. YH, QZ, and PW designed and fabricated the key device. YW, XX, ZD, and ZH conducted the experiments. YW and CL carried out the data processing. All the authors participated in the result analysis and discussion, and contributed to the writing of the manuscript. The author(s) read and approved the final manuscript.

Funding

National Science Fund for Distinguished Young Scholars (51722506); Tsinghua University Initiative Scientific Research Program (2021Z11GHX002); Shunde Core Technology Research Program (2130218003012); National key research and development program(2020YFC2200204).

Availability of data and materials
The datasets used and analysed during the current study are available from the corresponding author on reasonable request.

Declarations

Ethics approval and consent to participate
There is no ethics issue for this paper.

Consent for publication
All authors agreed to publish this paper.

Competing interests
The authors declare that they have no competing interests.

Received: 15 May 2022 Accepted: 20 August 2022
Published online: 30 September 2022

References

1. Coddington I, Swann WC, Nenadovic L, Newbury NR. Rapid and precise absolute distance measurements at long range. Nat Photonics. 2009;3(6):351–6. https://doi.org/10.1038/nphoton.2009.94.
2. Lu F, Milios E. Robot pose estimation in unknown environments by matching 2D range scans. J Intell Rob Syst. 1997;18(3):249–75. https://doi.org/10.1023/a:1007957421070.
3. Uttam D, Culshaw B. Precision time domain reflectometry in optical fiber systems using a frequency modulated continuous wave ranging technique. J Lightwave Technol. 1985;3(5):971–7. https://doi.org/10.1109/jlt.1985.1074315.
4. Trocha P, Kemal JN, Gaimard Q, Aubin G, Lelarge F, Ramdane A, et al. Ultra-fast optical ranging using quantum-dash mode-locked laser diodes. Sci Rep. 2022;12(1):1076. https://doi.org/10.1038/s41598-021-04368-4.
5. Mitchell EW, Hoehler MS, Giorgetta FR, Hayden T, Rieker GB, Newbury NR, et al. Coherent laser ranging for precision imaging through flames. Optica. 2018;5(8). https://doi.org/10.1364/optica.5.000988.
6. Levinson J, Askeland J, Becker J, Dolson J, Held D, Kammel S, et al. Towards Fully Autonomous Driving: Systems and Algorithms. IEEE Intelligent Vehicles Symposium (IV). 2011. p. 163–8. https://doi.org/10.1109/IVS.2011.5940562.
7. Steindorfer MA, Kirchner G, Koidl F, Wang P, Jilete B, Flohrer T. Daylight space debris laser ranging. Nat Commun. 2020;11(1):3735. https://doi.org/10.1038/s41467-020-17332-z.
8. Wang Z, Potsaid B, Chen L, Doerr C, Lee HC, Nielson T, et al. Cubic meter volume optical coherence tomography. Optica. 2016;3(12):1496–503. https://doi.org/10.1364/OPTICA.3.001496.
9. Ula RK, Noguchi Y, Iiyama K. Three-Dimensional Object Profiling Using Highly Accurate FMCW Optical Ranging System. J Lightwave Technol. 2019;37(15):3826–33. https://doi.org/10.1109/jlt.2019.2921353.
10. Lee J, Kim Y-J, Lee K, Lee S, Kim S-W. Time-of-flight measurement with femtosecond light pulses. Nat Photonics. 2010;4(10):716–20. https://doi.org/10.1038/nphoton.2010.175.
11. Martin A, Verheyen P, De Heyn P, Absil P, Feneyrou P, Bourderionnet J, et al. Photonic Integrated Circuit-Based FMCW Coherent LiDAR. J Lightwave Technol. 2018;36(19):4640–5. https://doi.org/10.1109/jlt.2018.2840223.
12. Dong Y, Zhu Z, Tian X, Qiu L, Ba D. Frequency-Modulated Continuous-Wave LIDAR and 3D Imaging by Using Linear Frequency Modulation Based on Injection Locking. J Lightwave Technol. 2021;39(8):2275–80. https://doi.org/10.1109/jlt.2021.3050772.
13. Hauser M, Hofbauer M. FPGA-Based EO-PLL With Repetitive Control for Highly Linear Laser Frequency Tuning in FMCW LIDAR Applications. IEEE Photonics J. 2022;14(1):1–8. https://doi.org/10.1109/jphot.2021.3139053.
14. Zhang F-M, Li Y-T, Pan H, Shi C-Z, Qu X-H. Vibration Compensation of the Frequency-Scanning-Interferometry-Based Absolute Ranging System. Applied Sciences. 2019;9(1). https://doi.org/10.3390/app9010147.
15. Cheng X, Liu J, Jia L, Zhang F, Qu X. Precision and repeatability improvement in frequency-modulated continuous-wave velocity measurement based on the splitting of beat frequency signals. Opt Express. 2021;29(18):28582–96. https://doi.org/10.1364/OE.433637.
16. Li B, Mo D, Wang P, Gan N, Lin M, Wang R, et al. FMCW lidar multitarget detection based on skeleton tree waveform matching. Appl Opt. 2021;60(27):8328–35. https://doi.org/10.1364/AO.431516.
17. Pan H, Qu X, Zhang F. Micron-precision measurement using a combined frequency-modulated continuous wave ladar autofocusing system at 60 meters standoff distance. Opt Express. 2018;26(12):15186–98. https://doi.org/10.1364/oe.26.015186.
18. Baumann E, Giorgetta FR, Deschenes JD, Swann WC, Coddington I, Newbury NR. Comb-calibrated laser ranging for three-dimensional surface profiling with micrometer-level precision at a distance. Opt Express. 2014;22(21):24914–28. https://doi.org/10.1364/OE.22.024914.
19. Hao Y, Song P, Wang X, Pan Z. A Spectrum Correction Algorithm Based on Beat Signal of FMCW Laser Ranging System. Sensors (Basel). 2021;21(15). https://doi.org/10.3390/s21155057.
20. Okano M, Chong C. Swept Source Lidar: simultaneous FMCW ranging and nonmechanical beam steering with a wideband swept source. Opt Express. 2020;28(16):23898–915. https://doi.org/10.1364/OE.396707.

21. Norgia M, Melchionni D, Pesatori A. Self-mixing instrument for simultaneous distance and speed measurement. Opt Lasers Eng. 2017;99:31–8. https://doi.org/10.1016/j.optlaseng.2016.10.013.
22. Zhang X, Kwon K, Henriksson J, Luo J, Wu MC. A large-scale microelectromechanical-systems-based silicon photonics LiDAR. Nature. 2022;603(7900):253–8. https://doi.org/10.1038/s41586-022-04415-8.
23. Norgia M, Magnani A, Pesatori A. High resolution self-mixing laser rangefinder. Rev Sci Instrum. 2012;83(4): 045113. https://doi.org/10.1063/1.3703311.
24. Lu C, Xiang Y, Gan Y, Liu B, Chen F, Liu X, et al. FSI-based non-cooperative target absolute distance measurement method using PLL correction for the influence of a nonlinear clock. Opt Lett. 2018;43(9):2098–101. https://doi.org/10.1364/OL.43.002098.
25. Mateo AB, Barber ZW. Multi-dimensional, non-contact metrology using trilateration and high resolution FMCW ladar. Appl Opt. 2015;54(19):5911–6. https://doi.org/10.1364/AO.54.005911.
26. Zhang K, Lv T, Mo D, Wang N, Wang R, Wu Y. Double sideband frequency scanning interferometry for distance measurement in the outdoor environment. Optics Communications. 2018;425:176–9. https://doi.org/10.1016/j.optcom.2018.04.056.
27. Ahmad Z, Liao Y-M, Kuo S-I, Chang Y-C, Chao R-L, Naseem, et al. High-Power and High-Responsivity Avalanche Photodiodes for Self-Heterodyne FMCW Lidar System Applications. IEEE Access. 2021;9:85661–71. https://doi.org/10.1109/access.2021.3089082.
28. Taimre T, Nikolic M, Bertling K, Lim YL, Bosch T, Rakic AD. Laser feedback interferometry: a tutorial on the self-mixing effect for coherent sensing. Advances in Optics and Photonics. 2015;7(3):570–631. https://doi.org/10.1364/aop.7.000570.
29. Giuliani G, Norgia M, Donati S, Bosch T. Laser diode self-mixing technique for sensing applications. Journal of Optics a-Pure and Applied Optics. 2002;4(6):S283–94. https://doi.org/10.1088/1464-4258/4/6/371.
30. Otsuka K. Self-mixing thin-slice solid-state laser Doppler velocimetry with much less than one feedback photon per Doppler cycle. Opt Lett. 2015;40(20):4603–6. https://doi.org/10.1364/ol.40.004603.
31. Lacot E, Day R, Stoeckel F. Coherent laser detection by frequency-shifted optical feedback. Physical Review A. 2001;64(4). https://doi.org/10.1103/PhysRevA.64.043815.
32. Zhu K, Guo B, Lu Y, Zhang S, Tan Y. Single-spot two-dimensional displacement measurement based on self-mixing interferometry. Optica. 2017;4(7). https://doi.org/10.1364/optica.4.000729.
33. Zhao Y, Zhu D, Chen Y, Tu Y, Bi T, Zhao Y, et al. All-fiber self-mixing laser Doppler velocimetry with much less than 0.1 pW optical feedback based on adjustable gain. Optics Letters. 2020;45(13):3565–8. https://doi.org/10.1364/ol.397819.
34. Otsuka K, Ohtomo T, Makino H, Sudo S, Ko JY. Net motion of an ensemble of many Brownian particles captured with a self-mixing laser. Appl Phys Lett. 2009;94(24):3. https://doi.org/10.1063/1.3156826.
35. Mowla A, Bertling K, Wilson SJ, Rakic AD. Dual-Modality Confocal Laser Feedback Tomography for Highly Scattering Medium. IEEE Sens J. 2019;19(15):6134–40. https://doi.org/10.1109/jsen.2019.2910122.
36. Gouaux F, Servagent N, Bosch T. Absolute distance measurement with an optical feedback interferometer. Appl Opt. 1998;37(28):6684–9. https://doi.org/10.1364/ao.37.006684.
37. Lu C, Liu G, Liu B, Chen F, Gan Y. Absolute distance measurement system with micron-grade measurement uncertainty and 24 m range using frequency scanning interferometry with compensation of environmental vibration. Opt Express. 2016;24(26):30215–24. https://doi.org/10.1364/OE.24.030215.
38. Hugon O, Lacot E, Stoeckel F. Submicrometric displacement and vibration measurement using optical feedback in a fiber laser. Fiber Integr Opt. 2003;22(5):283–8. https://doi.org/10.1080/01468030390221696.
39. Szwaj C, Lacot E, Hugon O. Large linewidth-enhancement factor in a microchip laser. Physical Review A. 2004;70(3). https://doi.org/10.1103/PhysRevA.70.033809.
40. Xu Z, Li J, Zhang S, Tan Y, Zhang X, Lin X, et al. Remote eavesdropping at 200 meters distance based on laser feedback interferometry with single-photon sensitivity. Optics and Lasers in Engineering. 2021;141. https://doi.org/10.1016/j.optlaseng.2021.106562.
41. Glombitza U, Brinkmeyer E. Coherent frequency-domain reflectometry for characterization of single-mode integrated-optical wave-guides. J Lightwave Technol. 1993;11(8):1377–84. https://doi.org/10.1109/50.254098.
42. Moore ED, McLeod RR. Correction of sampling errors due to laser tuning rate fluctuations in swept-wavelength interferometry. Opt Express. 2008;16(17):13139–49. https://doi.org/10.1364/oe.16.013139.
43. Jacquin O, Lacot E, Felix C, Hugon O. Laser optical feedback imaging insensitive to parasitic optical feedback. Appl Opt. 2007;46(27):6779–82. https://doi.org/10.1364/ao.46.006779.
44. Zhang Y, Hines AS, Valdes G, Guzman F. Investigation and Mitigation of Noise Contributions in a Compact Heterodyne Interferometer. Sensors (Basel). 2021;21(17). https://doi.org/10.3390/s21175788.
45. Deborah M. Kane, K. Alan Shore. Unlocking Dynamical Diversity: Optical Feedback Effects on Semiconductor Lasers. Chichester: John Wiley & Sons Ltd; 2005.
46. Tan Y, Zhang S, Zhang S, Zhang Y, Liu N. Response of microchip solid-state laser to external frequency-shifted feedback and its applications. Sci Rep. 2013;3:2912. https://doi.org/10.1038/srep02912.
47. Zhang X, Pouls J, Wu MC. Laser frequency sweep linearization by iterative learning pre-distortion for FMCW LiDAR. Opt Express. 2019;27(7):9965–74. https://doi.org/10.1364/OE.27.009965.
48. Zhao Y, Wang C, Zhao Y, Zhu D, Lu L. An all-fiber self-mixing range finder with tunable fiber ring cavity laser source. Journal of Lightwave Technology. 2020:1-. https://doi.org/10.1109/jlt.2020.3043331.
49. Zehao Y, Cheng L, Guodong L. FMCW LiDAR with an FM nonlinear kernel function for dynamic-distance measurement. Optics Express. 2022;30(11). https://doi.org/10.1364/oe.458235.
50. Zheng J, Jia L, Zhai Y, Ni L, Gu W, Sun Y, et al. High-Precision Silicon-Integrated Frequency-Modulated Continuous Wave LiDAR Calibrated Using a Microresonator. ACS Photonics. 2022. https://doi.org/10.1021/acsphotonics.2c00562.

51. Lacot E, Hugon O. Frequency-shifted optical feedback in a pumping laser diode dynamically amplified by a microchip laser. Appl Opt. 2004;43(25):4915–21. https://doi.org/10.1364/ao.43.004915.
52. Qin J, Zhou Q, Xie W, Xu Y, Yu S, Liu Z, et al. Coherence enhancement of a chirped DFB laser for frequency-modulated continuous-wave reflectometry using a composite feedback loop. Opt Lett. 2015;40(19):4500–3. https://doi.org/10.1364/OL.40.004500.
53. Wu H, Zhang F, Liu T, Balling P, Li J, Qu X. Long distance measurement using optical sampling by cavity tuning. Opt Lett. 2016;41(10):2366–9. https://doi.org/10.1364/OL.41.002366.

Publisher's Note